Available online at www.sciencedirect.com
SCIENCE DIRECT®
Journal of the European Ceramic Society 24 (2004) 3509–3520
www.elsevier.com/locate/jeurceramsoc

Statistical approach for minimizing cracks in combined flame spraying and laser surface modification of refractory ceramics

J. F. Li [a,b,*], L. Li [a], F. H. Stott [b]

[a] *Department of Mechanical, Aerospace and Manufacturing Engineering, Laser Processing Research Centre, University of Manchester Institute of Science and Technology (UMIST), P.O. Box 88, Manchester M60 1QD, UK*
[b] *Corrosion and Protection Centre, University of Manchester Institute of Science and Technology (UMIST), P.O. Box 88, Manchester M60 1QD, UK*

Received 25 May 2003; received in revised form 20 November 2003; accepted 28 November 2003

Available online 15 April 2004

Abstract

Combined flame and CO_2 laser spraying for surface modification of 20 wt.% Cr_2O_3–80 wt.% Al_2O_3 has been developed for improved surface performance of alumina-based refractory bricks. In this paper, the crack length per unit surface area and crack density of single treated tracks with respect to the three process parameters: laser irradiation intensity, powder feed rate and workpiece traverse velocity, have been investigated by employing a statistical approach involving statistical experiment design and regression analysis. It was found that the present statistical approach was effective for investigating the role of the process parameters on the crack length per unit surface area. Reducing both the powder feed rate and the workpiece traverse velocity could reduce the occurrence of cracks in the treated tracks. The former corresponded to decreasing the α-Al_2O_3 content in the treated tracks, and the latter to decreasing the cooling and solidifying rate of the melt pool.

Keywords: Flame spraying; Laser spraying; Refractories; Mullite; Crack growth

1. Introduction

Aluminosilicate refractories account for the majority of high-temperature ceramic materials used as furnace and incinerator linings in the glass melting, cement, ceramic and, especially, the iron and steel industries.[1] Generally, the refractories are fabricated using conventional powder processing and have microstructures consisting of aggregates, several millimeters in size and a bond matrix of finer grains and/or glass. A certain amount of porosity is often deliberately included in the refractories to improve heat insulation.[2] In addition, some cracks often occur in such refractories.

Technological advances in the various industries have resulted in a demand for higher grade refractories for use in more severe conditions.[1] Also, higher grade refractories obviously have longer service life than conventional refractories under identical conditions. The choice of a refractory lining for a particular application must take into account both the high-temperature properties and cost.[2] As the refractories are often attacked preferentially on the surfaces by penetration of environmental species, for example, molten slag penetration, and corrosion, improving surface performance of conventional refractories by surface engineering methods could be a cost-effective approach for giving improved performance of such refractories. In recent years, laser surface melting has been used to improve the surface properties of conventional aluminosilicate refractories, with emphasis on sealing surface pores and cracks, thus enhancing penetration and corrosion resistance.[2–4] During such laser surface processing of ceramic materials, some innovations have been required to the conventional laser surface melting for decreasing and, even, eliminating cracks due to thermal-induced stresses. For example, Bradley et al.[2] developed flame-assisted laser processing to reduce thermal stress and successfully achieved crack-free and dense laser-treated surface layers on several aluminosilicate refractories. Triantafyllidis et al.[3,4] used two combined laser sources to control the thermal gradients and cooling rates during laser surface melting of similar refractories and effectively eliminated the occurrence of cracks.

* Corresponding author. Tel.: +44-161-200-3827; fax: +44-161-200-3803.
E-mail address: j.li-3@umist.ac.uk (J.F. Li).

0955-2219/$ – see front matter © 2004 Elsevier Ltd. All rights reserved.
doi:10.1016/j.jeurceramsoc.2003.11.021

In addition to dense surface layers, chemical surface modification should also be important for further improving the surface performance of conventional refractories. Extensive research has been conducted into the effects of refractory compositions on slag melt corrosion, and shown that the dissolution and chemical degradation of such materials are clearly associated with the compositions of both the refractory and the slag.[5] For example, Sandhage and Yurek[6] investigated the dissolution of $(Al,Cr)_2O_3$ in MgO-containing lime–alumina–silica slag melts at 1550 °C. They found that, with sufficient MgO in the melt, or sufficient Cr_2O_3 in the $(Al,Cr)_2O_3$, an $Mg(Al,Cr)_2O_4$ spinel solution layer formed at the $(Al,Cr)_2O_3$/melt interface. This inhibited directional dissolution of the $(Al,Cr)_2O_3$ in the slag melt and, hence, improved the corrosion resistance.

In the present investigation, a process combining flame spraying and simultaneous CO_2 laser surface treatment has been developed for improving the surface integrity of an aluminosilicate refractory, giving a relatively dense structure and chemical modification. Flame spraying was a useful heating source for increasing the process velocity and controlling the temperature gradients and thermal stresses during surface processing of the refractory. Compared with the earlier method involving laser surface melting of similar aluminosilicate refractories,[2–4] an apparent advantage of the present process is that a chemical modification of the refractory surface is accomplished by flame spraying a higher grade powder material, consisting of 20% Cr_2O_3 and 80% Al_2O_3 by weight. For such a novel process, it is critical to set up an appropriate combination between the flame spraying parameters and the laser treating parameters in order to achieve dense surface layers, free of pores and cracks and with stable phase constituents. In this paper, a statistical approach, involving statistical experiment design and regression analysis, is shown to be an efficient method for optimizing the process parameters, in order to decrease the extent of crack formation during surface processing. For the experimental programme, single tracks, treated using the combined process, were selected in order to avoid the complicated physical and chemical processes introduced by heating effects due to overlaps between adjacent treated tracks. Phase and microstructure analyses of some of the treated tracks were also carried out in order to correlate the occurrence of cracks with characteristics of the material.

2. Experimental procedures

2.1. Flame spray feedstock and workpiece materials

The feedstock for the flame spray process was a mechanically blended powder of 20% Cr_2O_3 and 80% Al_2O_3 by weight. The former was the FST C-604.22 powder (Flame Spray Technologies b. v., Netherlands), a type of fused and crushed chromium oxide powder, eskolaite, with particle size $-45+10\,\mu m$. The latter was the Sulzer-Metco 105SFP powder (Sulzer-Metco, Switzerland), a type of fused and crushed alumina powder, α-Al_2O_3 plus small amount of β-Al_2O_3, with particle size $-25+5\,\mu m$ (Fig. 1). The workpiece was a 60% alumina-based refractory ceramics provided by Cleanaway Ltd. in the form of bricks approximately 200 mm × 200 mm × 100 mm, typically used to line furnaces and incinerators. It contains 60.0% Al_2O_3, 35.0% SiO_2, 1.6% P_2O_5, 1.4% TiO_2, 0.9% Fe_3O_4, 0.3% MgO, 0.3% Na_2O, 0.2% K_2O and 0.2% CaO by weight, and is mainly mullite with some cristobalite. For the purpose of experimental convenience, the as-received refractory brick was sectioned into squares, 80 mm × 50 mm × 20 mm, prior to surface treatment. Cracks and open surface pores, as well as mullite aggregates, 1–4 mm in size are visible on the sectioned surface (Fig. 2). Fig. 3 presents X-ray diffraction (XRD) spectra for both the feedstock powder and the refractory brick. The XRD spectrum of the latter was collected from particles, smaller than 100 μm, following manual crushing and milling of a brick using an alumina mortar.

Fig. 1. A typical secondary electron scanning electron micrograph of the mechanically blended powder (20% Cr_2O_3 and 80% Al_2O_3 by weight).

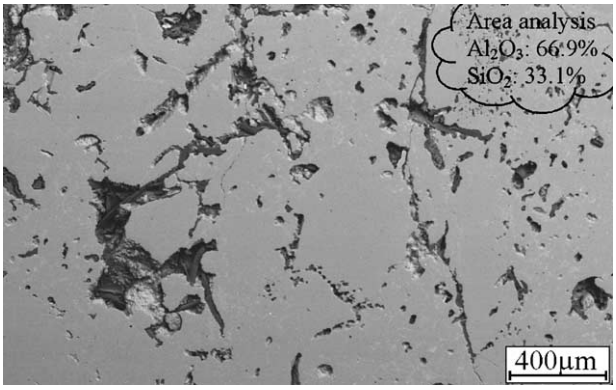

Fig. 2. A representative back scattered scanning electron micrograph of a polished section, showing the morphologies of pores and cracks within the refractory brick, the callout presents the EDX results from quantitative analysis, by weight.

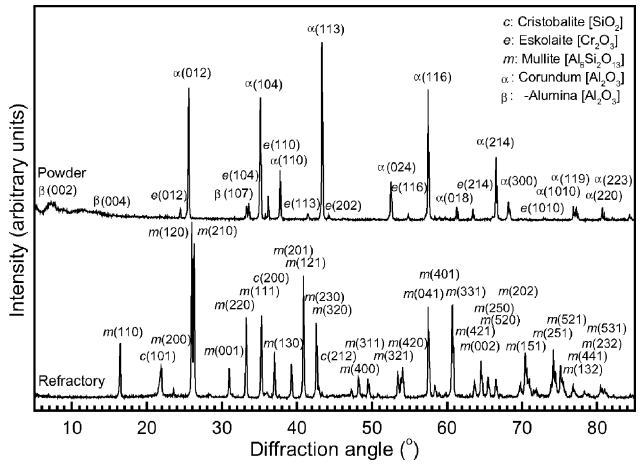

Fig. 3. XRD spectra for the feedstock powder and the refractory brick, identifying their phase constituents.

2.2. The combined process and statistical experiment

The combined process set up comprised a Sulzer-Metco Type 6P-II thermospray gun and a Rofin-Sinar CO_2 laser (Rofin-Sinar, Germany) emitting at 10.6 μm and operating in the continuous wave (CW) TEM_{01}* mode, with a maximum output power of 1.2 kW (Fig. 4). Feedstock powder particles used for chemical surface modification are injected into the flame jet where they are partially melted and propelled towards a workpiece surface moving at a certain traverse velocity, to produce a coating. At the same time, a continuous CO_2 laser, with sufficient intensity, is incident on the produced coating, leading to the formation of a melt pool, due to a very intensive heat flux. The melt pool then solidifies to produce a dense treated track.

For such a combined process, the quality of the treated track on the refractory surface is influenced by a number of process parameters, including laser power, beam profile, spot size, flame burning gas, spray distance, jet angle, powder gas flow, powder feed rate and workpiece traverse velocity, as well as the position of the workpiece on which the flame jet impinges relative to the laser incidence. As most of the process parameters are interdependent, only three parameters: laser power, powder feed rate and workpiece traverse velocity, were varied and investigated, while the other parameters were fixed following initial trials. In addition, in order to avoid the complicated physical and chemical processes introduced by the heating effect of overlaps between adjacent treated tracks, only single tracks have been used in the present investigation.

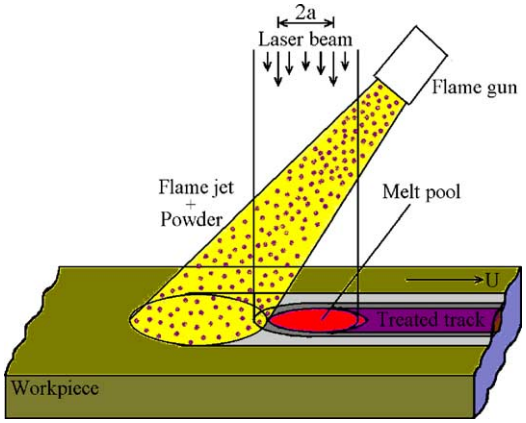

Fig. 4. Schematic diagram showing the combined process set up for flame spraying and laser surface treating.

A relatively new statistical experiment method, the uniform design experiment, has been employed to decrease the number of experimental trials of the three process parameters. The uniform design experiment method was developed by Fang and Wang,[7] based on the number theory. Its aim is to replace the full spectrum of combined trials involving the experimental parameters by relatively fewer experimental trials uniformly distributed across the scope of the experimental parameters. These trials are determined by the number-theoretic method and have been mathematically proved to be a good approximation to a full spectrum of the experimental parameters. The tables for arranging various experiment trials have been listed in the reference.[7] Compared with conventional statistical methods, such as the Taguchi and orthogonal design methods,[8,9] this statistical experiment method decreases further the number of trials for processes involving a large number of factors and graded into larger numbers of factor levels.

The experimental trials for the three investigated process parameters were arranged according to Table $U_{10}(10^2 5)$ of the uniform design experiment, as listed in Table 1. The design scopes of the three process parameters were determined from several preliminary experiments, ensuring that visible melt pools were produced for all the trials. In Table 1, the laser power and powder feed rate were graded into 10 levels, while the workpiece traverse velocity was graded into five levels. The three parameters, graded into the 10 and 5 levels, were arranged into 10 experimental trials. With the other process parameters fixed, the laser beam had a circular beam with cross-sectional geometry of 16 mm diameter. It is

Table 1
The investigated process parameters for experimental trials designed according to a Table $U_{10}(10^2 5)$ of the uniform design experiment

Experimental trial	Laser power, x_1 (W)	Powder feed rate, x_2 (g/min)	Workpiece traverse velocity, x_3 (mm/s)
UP0800F05V5	800	3.2	5
UP0950F10V5	950	6.4	5
UP1100F15V4	1100	9.6	4
UP0700F20V4	700	12.8	4
UP0850F25V3	850	15.5	3
UP1000F04V3	1000	2.6	3
UP1150F07V2	1150	4.8	2
UP0750F12V2	750	8.0	2
UP0900F17V1	900	11.2	1
UP1050F22V1	1050	14.1	1

known that a larger laser beam can decrease the temperature gradient and cooling rate during processing by providing a larger incident area and a longer heating time when compared with a smaller laser beam. Thus, a large laser beam should help to achieve stable phase constituents and reduce thermal-induced stresses. The flame spraying method used acetylene and oxygen, and the gas flow rates were as recommended by Sulzer-Metco for spraying alumina powder 105SFP, i.e. an acetylene flow rate of 50 l/min under a pressure of 1.0 bar and an oxygen flow rate of 42 l/min under a pressure of 2.1 bar. The flame jet center, 130 mm from the flame gun nozzle, impinged on the workpiece surface approximately 20 mm ahead of the laser beam center to avoid the molten materials in the melt pools from being blown away by the dynamic flame jet. The spray angle of the flame jet impinging on the workpiece surface was 60°, while the laser beam was perpendicular to the surface. The feedstock powder was delivered into the flame jet using a Praxair powder feeder (Praxair Thermal Spray Products, Model 1264, USA) with an argon gas flow of 8 l/min as carrier gas. The workpiece specimens were driven by an *x–y* CNC table.

The process optimization has focused on decreasing the occurrence of cracks in the treated tracks. The occurrence of cracks in the treated tracks were directly associated with thermal-induced and/or residual stresses. However, these thermal-induced and/or residual stresses would release to a certain degree as soon as they went beyond the crack strength. Therefore, the residual stress measurement was impracticable for the process optimization, and the present work would pay attention to observation and measurement of the resulting cracks on the treated tracks. Cracks formed during laser surface melting of ceramics are usually oriented either parallel and perpendicular to the workpiece surface.[2] Observation and measurement of the cracks on the as-treated surfaces of the single tracks were carried out using a KYOWA optical stereomicroscope (KYOWA OPTICAL Model SD-2PL, Japan) at a magnification of 10×. Fig. 5 presents an optical stereomicroscope image of an as-treated surface of a sample, showing the crack morphology. It should be noted that such observations and measurements are only valid for cracks oriented perpendicular to the workpiece surface, but not for cracks oriented parallel to the workpiece surfaces. Fortunately, no obvious cracks oriented parallel to the workpiece surfaces were observed in the cross sections of the treated tracks, cut using a Struers Accutom-5 cutting machine (Struers, Germany). For comparison between experimental trials, the measured crack data were expressed as crack length per unit surface area (L_C) and crack density (D_C) for every treated track, according to Eqs. (1) and (2), respectively.

Fig. 5. An optical stereomicroscope image of the as-treated track of sample UP0850F25V3, showing the crack morphology.

$$L_C = \frac{\sum_{i=1}^{n} L_i}{L \times W} \tag{1}$$

$$D_C = \frac{n}{L \times W} \tag{2}$$

where L_i ($i = 1, \ldots, n$) are the length data, and n is the total number of cracks measured on a treated track surface; L and W are, respectively, the length and width of the treated track surface.

The crack length per unit surface area and crack density values, which are correlated with the investigated process parameters, the laser power, powder feed rate and workpiece velocity, can be expressed using the following polynomial equation:[10]

$$F(x_1, x_2, x_3) = \sum_{i=1}^{3} x_i + \sum_{i=1}^{3}\sum_{i<j}^{3} x_i x_j + \cdots + \sum_{i=1}^{3}\sum_{i<j}^{3} x_i^{m-1} x_j + \sum_{i=1}^{3} x_i^m \tag{3}$$

where $F(x_1, x_2, x_3)$ is the crack length per unit surface area or crack density; x_1, x_2, x_3 stand for the laser power, powder feed rate and workpiece velocity, respectively, and m is the order of the polynomial equation: a value of m equal to 1 is generally used as the simple linear regression model; a value of m equal to 2 is sometimes used as the quadratic model for better fitting of experimental data. In the present analysis, m values of both 1 and 2 were used and compared.

Once the data for the crack length per unit surface area and crack density from the experimental trials are obtained, the polynomial equations relating to the investigated process parameters can be established by regression analysis. However, in the uniform design experiment, the total number of the experimental trials, 10, in Table 1, is too small to regress directly the experimental results to Eq. (3) with an order of m more than 1. Thus, the items in Eq. (3) that negligibly influence the crack length per unit surface area or crack density should be removed, and only those that are statistically significant to the crack length per unit surface area or crack density are retained in the regressed equations.[7] The methods to sift the items include the best subset regression, the

Table 2
The investigated process parameters for experimental trials to evaluate whether or not the present statistical approach is valid for optimizing the process parameters

Experimental trial	Laser power, x_1 (W)	Powder feed rate, x_2 (g/min)	Workpiece traverse velocity, x_3 (mm/s)
CP0900F10V1	900	6.4	1
CP0850F05V1	850	3.2	1
CP1000F05V1	1000	3.2	1
CP0600F05V1	600	3.2	1
CP1200F20V5	1200	12.8	5
CP1200F05V5	1200	3.2	5
CP1200F05V1	1200	3.2	1
CP1200F05V2	1200	3.2	2
CP1200F05V3	1200	3.2	3
CP1200F05V4	1200	3.2	4
CP1000F05V4	1000	3.2	4

backward elimination procedure, the stepwise regression, etc.[11] In the present investigation, the stepwise regression method was used, with a self-developed program based on the Statistics Toolbox of MATLAB Version 6.0.0.88 (R12) on PCWIN (Mathworks Inc.).

In addition to the experimental trials for the uniform design experiment listed in Table 1, several experimental trials were also carried out within the design scopes of the three process parameters, as listed in Table 2. The resulting crack length per unit surface area and crack density data were further regressed as renewed polynomial equations for the investigated process parameters. This could be considered as a measure to evaluate whether the present statistical approach is valid for optimizing the combined process parameters with emphasis on decreasing the amount of cracking.

2.3. Phase identification and microstructure observation

Phase identification and microstructural observation of some representative treated tracks were carried out in order to correlate the occurrence of the cracks with material characteristics, as well as with the investigated process parameters. The phases in the as-treated surfaces of the single tracks were identified using XRD. The data were collected using a Philip X'pert APD, PW3710 diffractometer (Philips Co., Netherlands). The experimental conditions included, a Cu target, operated at 50 kV and 40 mA, 0.5° automatic divergent slit and 0.05 mm receiving slit. The collected data angles ranged from 5.025 to 84.975° in 2θ with a step size of 0.05° and a counting time of 2 s per step.

The microstructural observation and element analysis were performed on polished cross sections of the treated tracks using a scanning electron microscope (SEM) consisting of an AMRAY 1810 SEM and ISIS X-ray microanalysis (EDX) workstation. For preparation of the polished cross sections, the samples were first cut to the required dimensions, 28 mm × 10 mm × 5 mm, and then mounted using epoxy resin. The mounted samples were successively ground with Struers MD-Piano 220 and MD-Allegro (with diamond slurry of 15 μm in size) for 5 and 10 min and, finally polished using MD-Plan and MD-Dac clothes with diamond slurries of 6 and 3 μm for 15 and 60 min, respectively.

3. Results

3.1. Stepwise regression analysis

Table 3 lists the results of the stepwise regression analysis in which the crack lengths per unit surface area of the treated tracks for the uniform design experiment were regressed as the first and second order polynomial equations of the investigated three process parameters: laser power, powder feed rate and workpiece traverse velocity. Whether a regressed equation is statistically significant is judged from the confidence level determined from the over F-value and the regression and residual degrees of freedom.[11] The closer to unity is the confidence level, the more significant is the regressed equation. The precision of the prediction for the equation is determined from the residual mean square value, e.g. if the process parameters are x_1, x_2 and x_3, there would be a probability of 0.95 that the predicted objective function, here the crack length per unit surface area, is within $F(x_1, x_2, x_3) \pm 2(\text{residual mean square})^{1/2}$.[11] From Table 3, it can be seen that both the first and second order regressed equations are statistically significant with confidence levels higher than 0.95. The second order regressed equation has improved both the significance and prediction precision when compared with the first order regressed equation. The second order equation has a confidence level of 0.99 and a prediction error of $\pm 0.06\,\text{mm/mm}^2$. According to the second order equation, the crack length per unit surface area is influenced by the laser power, the powder feed rate and the workpiece traverse velocity. The higher is the laser power and the lower are the powder feed rate and the workpiece traverse velocity, the lower is the crack length per unit surface area.

Table 3
Results for the stepwise regression analysis in which the crack lengths per unit surface area of the treated tracks of the uniform design experiment were regressed as both the first and second order polynomial equations of the investigated process parameters

Order	Equation	Source	Degrees of freedom	Mean square	Overall F	Confidence level
1	$4.10 \times 10^{-1} - 3.09 \times 10^{-4}x_1 + 5.66 \times 10^{-3}x_2$	Regression	2	1.50×10^{-2}	5.90	0.97
		Residual	7	2.55×10^{-3}		
2	$3.55 \times 10^{-1} - 3.78 \times 10^{-4}x_1 + 1.05 \times 10^{-1}x_3 + 4.76 \times 10^{-6}x_1x_2 - 1.04 \times 10^{-2}x_3^2$	Regression	4	1.09×10^{-2}	12.26	0.99
		Residual	5	8.87×10^{-4}		

Table 4
Results for the renewed stepwise regression analysis of the crack length per unit surface area, in which the crack data of the experimental trials were merged with those of the uniform design experiment

Order	Equation	Source	Degrees of freedom	Mean square	Overall F	Confidence level
1	$2.19 \times 10^{-1} - 1.17 \times 10^{-4}x_1 + 4.64 \times 10^{-3}x_2 + 1.45 \times 10^{-2}x_3$	Regression	3	9.55×10^{-3}	2.31	0.89
		Residual	17	4.14×10^{-3}		
2	$9.97 \times 10^{-1} - 1.74 \times 10^{-3}x_1 + 8.57 \times 10^{-7}x_1^2 + 1.79 \times 10^{-3}x_2x_3$	Regression	3	1.52×10^{-2}	4.81	0.99
		Residual	17	3.15×10^{-3}		

Table 4 presents the results for the renewed stepwise regression analysis of the crack length per unit surface area, in which the crack data from the experimental trials, listed in Table 2, were merged with those from the uniform design experiment. The renewed first order equation has a relatively low significance, with a confidence level of 0.89. As for the results listed in Table 3, the renewed second order regressed equation in Table 4 also has higher significance and prediction precision than the first order regressed equation. The renewed second order regressed equation is statistically significant, with confidence levels of 0.99. The second regressed equations, listed in Tables 3 and 4, both indicate that the crack length per unit surface area decreases with decrease in powder feed rate and workpiece traverse velocity. Furthermore, the renewed second order equation in Table 4 shows that, under low powder feed rate and workpiece traverse velocity, the crack length per unit surface area decreases to a minimum value of 0.11 mm/mm^2 with increasing the laser power up to 1015 W, then increases with further increase in the laser power. Fig. 6 presents a graph showing the crack length per unit surface area as a function of laser power, at the powder feed rate of 3.2 g/min and workpiece traverse velocity of 1 mm/s. Although the prediction error for the renewed second order equation has increased to $\pm$0.10 mm/mm^2, it should be acceptable for predicting disordered systems, such as cracks. Table 5 compares the experimental crack length per unit surface area with the value calculated from the renewed second order regressed equation. They are in reasonable agreement with each other for all the experimental trials.

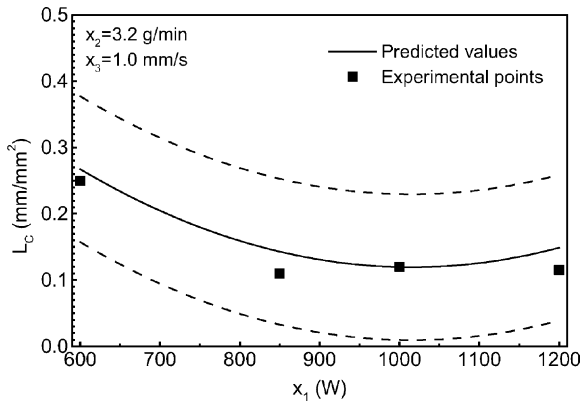

Fig. 6. Crack length per unit surface area, L_C, as a function of laser power, x_1, at the powder feed rate of 3.2 g/min and workpiece traverse velocity of 1 mm/s. Note that the dash lines stand for the prediction error with a probability of 0.95.

Table 6 lists the results for the stepwise regression analysis in which the crack densities of the treated tracks from the uniform design experiment were regressed as the first and second order polynomial equations of the investigated process parameters. Table 7 lists the results for the renewed stepwise regression analysis of the crack density, in which the crack data from the experimental trials, listed in Table 2, were merged with those of the uniform design experiment. Both the first and second order equations listed in Table 6 are statistically significant and have high prediction precision. However, once the crack density data from the experimental trials listed in Table 2 are incorporated into those of the uniform design experiment, not only do the statistical significance and prediction precision of the regressed equations obviously decrease, but, also, the effects of the investigated process parameters on the crack density show different and, even, contrary trends. The second order equation in Table 6 shows that the crack density decreases with increase in both the laser power and the workpiece traverse

Table 5
Comparison of the experimental crack lengths per unit surface area with the values calculated from the renewed second order regressed equation listed in Table 4

Experimental trial	Experimental value (mm/mm^2)	Value from the second order equation (mm/mm^2)	Relative error (%)
UP0800F05V5	0.14	0.18	26.7
UP0950F10V5	0.11	0.17	60.7
UP1100F15V4	0.12	0.19	59.0
UP0700F20V4	0.26	0.29	13.3
UP0850F25V3	0.30	0.22	−26.1
UP1000F04V3	0.14	0.14	5.7
UP1150F07V2	0.28	0.20	−28.1
UP0750F12V2	0.15	0.14	−2.0
UP0900F17V1	0.13	0.14	10.6
UP1050F22V1	0.13	0.13	−2.7
CP0900F10V1	0.16	0.14	−13.4
CP0850F05V1	0.11	0.14	25.1
CP1000F05V1	0.12	0.12	−2.3
CP0600F05V1	0.25	0.27	6.7
CP1200F20V5	0.26	0.26	−2.2
CP1200F05V5	0.32	0.17	−47.5
CP1200F05V1	0.11	0.15	28.5
CP1200F05V2	0.12	0.15	22.5
CP1200F05V3	0.14	0.16	12.7
CP1200F05V4	0.14	0.16	21.3
CP1000F05V4	0.17	0.14	−20.6

Table 6
Results for the stepwise regression analysis in which the crack densities of the treated tracks of the uniform design experiment were regressed as the first and second order polynomial equations of the investigated process parameters

Order	Equation	Source	Degrees of freedom	Mean square	Overall F	Confidence level
1	$1.02 \times 10^{-1} - 6.81 \times 10^{-5}x_1 - 4.90 \times 10^{-3}x_3$	Regression	2	5.52×10^{-4}	4.31	0.94
		Residual	7	1.28×10^{-4}		
2	$1.24 \times 10^{-1} - 1.16 \times 10^{-4}x_1 +$ $1.60 \times 10^{-5}x_1x_3 - 3.27 \times 10^{-3}x_3^2$	Regression	3	5.10×10^{-4}	6.54	0.97
		Residual	6	7.81×10^{-5}		

Table 7
Results for the renewed stepwise regression analysis of the crack density, in which the crack data for the complemented experimental trials were merged with those of the uniform design experiment

Order	Equation	Source	Degrees of freedom	Mean square	Overall F	Confidence level
1	$1.24 - 6.51 \times 10^{-2}x_2$	Regression	1	1.60	1.64	0.78
		Residual	19	9.78×10^{-1}		
2	$1.16 - 2.74 \times 10^{-1}x_2 + 2.29 \times 10^{-4}x_1x_2$	Regression	2	1.71	1.83	0.81
		Residual	18	9.31×10^{-1}		

velocity, and is not significantly influenced by the powder feed rate. However, the renewed second order equation in Table 7 shows that the crack density increases with increasing laser power and decreasing powder feed rate, and is not significantly influenced by the workpiece traverse velocity. Consequently, there is an apparent difference between the experimental crack density and the value predicted from the renewed regressed equations (Table 8).

3.2. Phase identification

Fig. 7 shows the XRD spectra for several representative treated tracks. From these spectra, it is evident that a lower laser power and/or a larger powder feed rate lead to the resulting treated tracks consisting mainly of α-Al_2O_3, with smaller amounts of eskolaite (CP0600F05V1 and CP0900F10V1). With increase in laser power, the resulting treated tracks are mainly comprised of mullite with some cristobalite and α-Al_2O_3 (CP0850F05V1 and CP1000F05V4). With further increase in laser power, cristobalite and α-Al_2O_3 in the corresponding treated tracks are decreased and, even, eliminated (CP1000F05V1 and CP1200F05V4). For identical laser power and powder feed rate, a faster workpiece traverse velocity results in a

Table 8
Comparison of the experimental crack densities with values calculated from the renewed second order regressed equation listed in Table 7

Experimental trial	Experimental value (1/mm^2)	Value from the second order equation (1/mm^2)	Relative error (%)
UP0800F05V5	0.015	0.871	5771.5
UP0950F10V5	0.012	0.800	6695.2
UP1100F15V4	0.014	0.947	6681.4
UP0700F20V4	0.028	−0.292	−1151.3
UP0850F25V3	0.039	−0.071	−282.3
UP1000F04V3	0.019	1.109	5804.5
UP1150F07V2	0.060	0.344	476.4
UP0750F12V2	0.021	0.400	1770.8
UP0900F17V1	0.019	0.683	3529.9
UP1050F22V1	0.015	1.046	6883.9
CP0900F10V1	1.117	0.727	−34.9
CP0850F05V1	0.711	0.908	27.7
CP1000F05V1	1.110	1.017	−8.4
CP0600F05V1	2.974	0.725	−75.6
CP1200F20V5	2.788	1.167	−58.2
CP1200F05V5	2.966	1.163	−60.8
CP1200F05V1	0.713	1.163	63.2
CP1200F05V2	0.892	1.163	30.5
CP1200F05V3	1.246	1.163	−6.7
CP1200F05V4	1.132	1.163	2.8
CP1000F05V4	1.323	1.017	−23.1

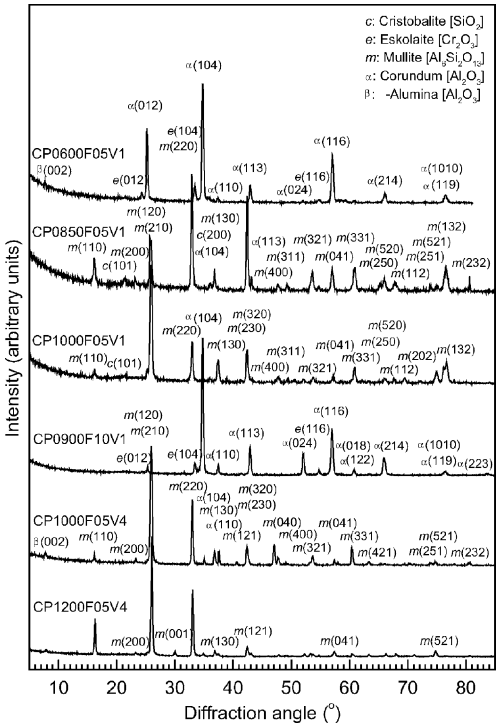

Fig. 7. XRD spectra for several representative treated tracks, identifying their phase constituents.

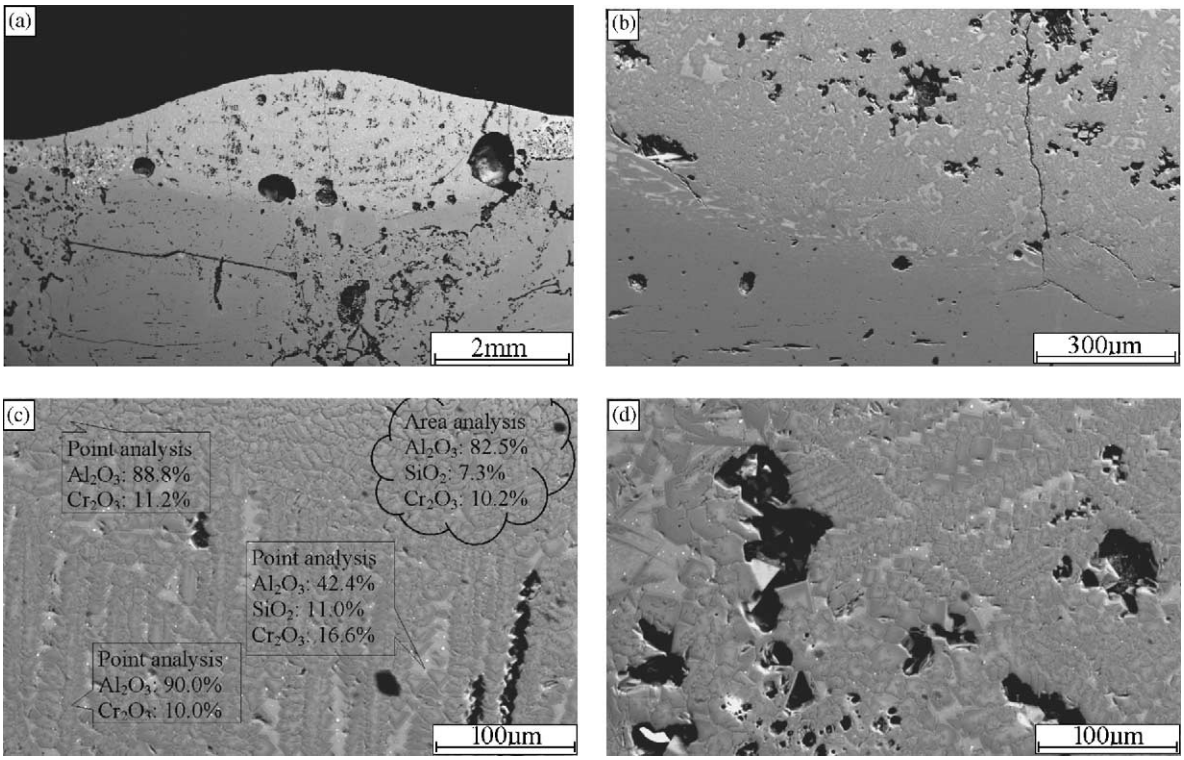

Fig. 8. Back scattered scanning electron micrographs of a polished cross section of sample, CP0600F05V1: (a) whole view, (b) melt/substrate interface, (c) cellular/dendritic structure, relatively dense region; the callouts present the EDX results of quantitative analysis by weight, (d) another relatively porous region.

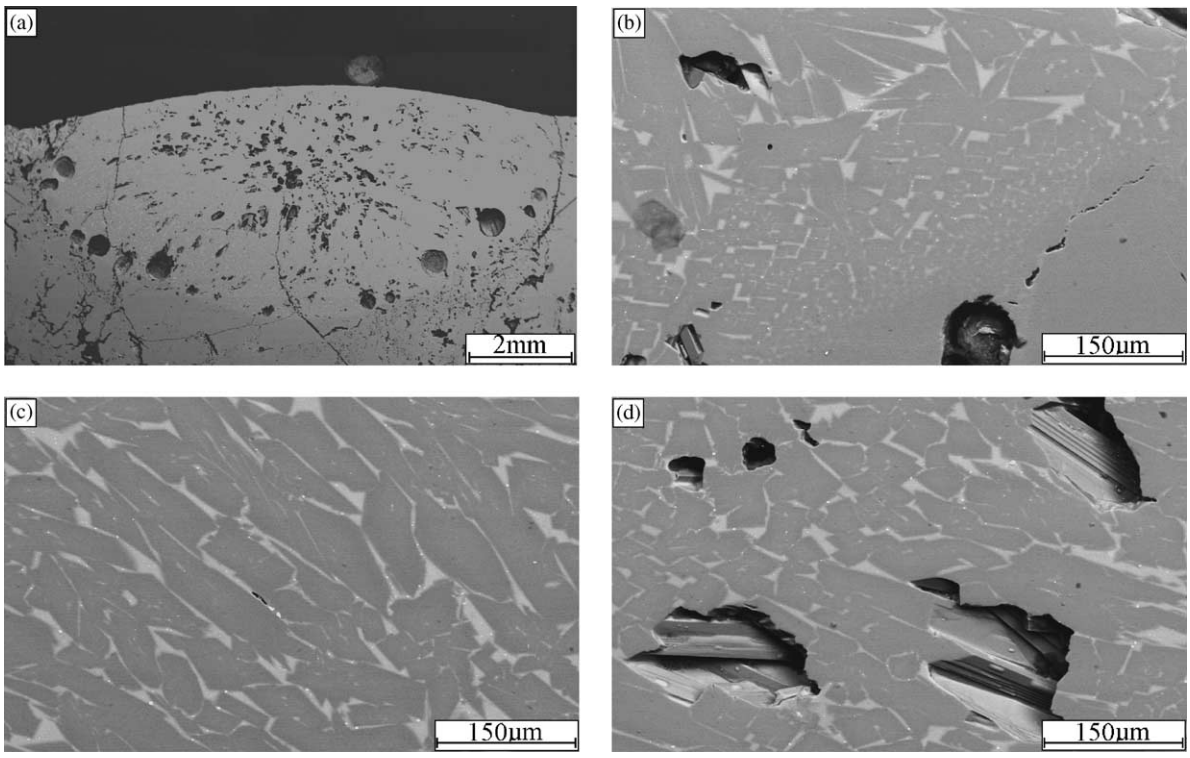

Fig. 9. Back scattered scanning electron micrographs of a polished cross section of sample, CP1000F05V1: (a) whole view, (b) melt/substrate interface, (c) elongated mullite grains, between which a eutectic Al_2O_3, SiO_2 and Cr_2O_3 is observed, relatively dense region, (d) another relatively porous region, elongated mullite grains interlocked together are clearly observed.

relatively lower amount of α-Al_2O_3 in the treated track than a slower workpiece traverse velocity (CP1000F05V4 and CP1000F05V1). In addition, there exists a small amount of β-Al_2O_3 in some treated tracks; this can be attributed to some partially molten feedstock particles embedded within these tracks during the processing.[12]

3.3. Microstructure observation

Observations using the SEM revealed that the microstructural morphologies of the treated tracks could be clearly correlated with their phase compositions. In the case where α-Al_2O_3 is the main phase, the treated tracks exhibit the typical cellular/dendritic microstructures of materials produced by rapid solidification processing, consisting of cellular/dendritic α-Al_2O_3 grains and a small amount of a white phase, between cellular/dendritic α-Al_2O_3 grains. It is difficult to identify the white phase. According to the XRD and EDX results and referring to the SiO_2–Al_2O_3 and Al_2O_3–Cr_2O_3 phase diagrams,[17,18] the white phase may be the eutectic Al_2O_3, SiO_2 and Cr_2O_3 (Figs. 7 and 8). For cases where mullite is the main phase, the treated tracks are comprised of elongated mullite grains, interlocked together, with small amounts of white phase between the interlocked grains (Figs. 9 and 10). Again, the white phase may be the eutectic Al_2O_3, SiO_2 and Cr_2O_3. Under identical laser power and powder feed rate, a faster workpiece traverse velocity tends to produce relatively finer mullite grains in addition to smaller melt tracks (Fig. 10) than a slower workpiece traverse velocity (Fig. 9). In addition, in Figs. 8–10, it can be seen that there exists gradual transition regions around the melt/substrate interfaces, large pores along the interfaces or within the treated surface layers as well as a few cracks vertical to the surface. The results of EDX quantitative analysis indicate that the amounts of Al_2O_3 in the treated surface layers are increased compared with the amount of the as-received refractory brick (Fig. 2).

4. Discussion

Cracks in materials belong to disordered systems[13] and, thus, are difficult to be quantitatively related to material process parameters. In order to optimize the process parameters, investigations of the laser surface melting of various ceramic materials[2,14,15] have characterized thermally induced cracks in terms of crack length, width, density, direction and morphology as well as the thickness of the corresponding treated layers. In contrast, the present optimized process using the statistical approach has simply considered the cracks in terms of crack length per unit surface area and crack density. In particular, this requires fewer experimental trials than previous investigations[2,14,15] for similar ranges of process parameters. It should be stated

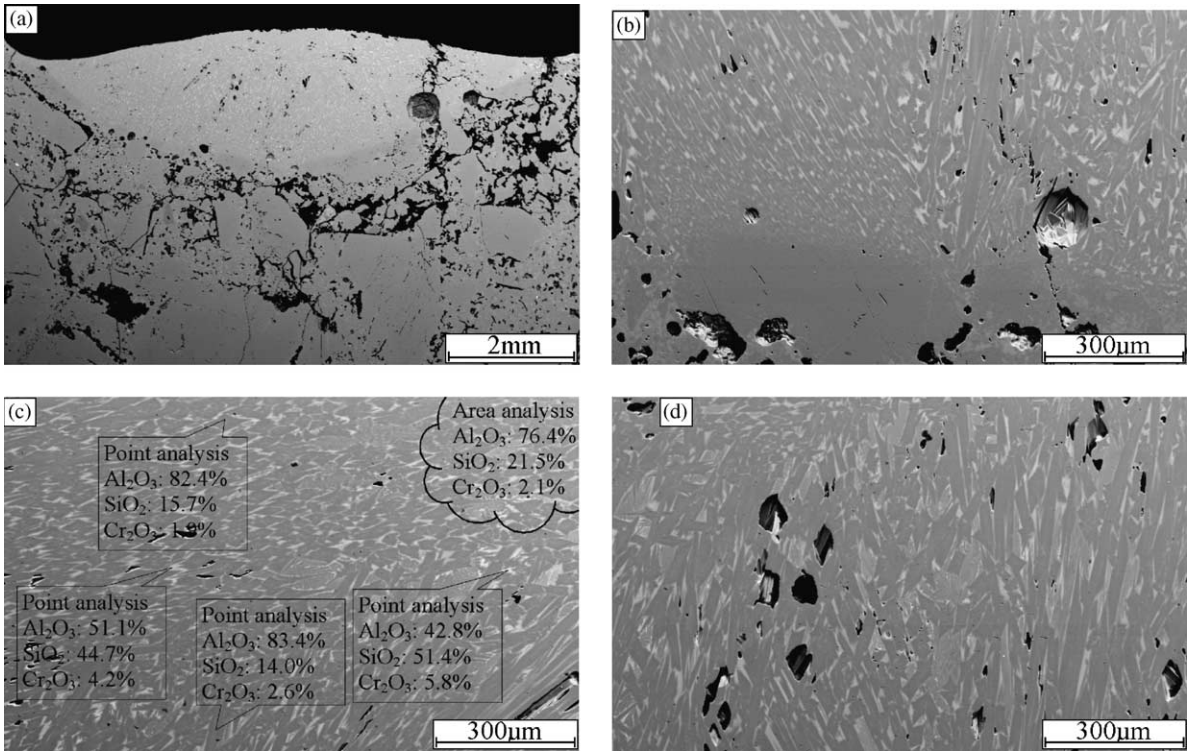

Fig. 10. Back scattered scanning electron micrographs of a polished cross section of sample, CP1000F05V4: (a) whole view, (b) melt/substrate interface, (c) elongated mullite grains, between which a eutectic Al_2O_3, SiO_2 and Cr_2O_3 is observed, relatively dense region; the callouts present the EDX results of quantitative analysis by weight, (d) another relatively porous region.

that the present statistical approach has not been used to develop models, but mainly to predict the effects of the process parameters on the occurrence of cracks. The results obtained show that the present statistical approach is valid for optimizing the process parameters needed to obtain a reduction in the occurrence of cracks when the crack length per unit surface area is chosen as the objective function, but is not valid when the crack density is the objective function.

The validity of the former can be justified from the following facts: the trends in the crack length per unit surface area as a function of the investigated process parameters reflected by the regressed second order polynomial equation listed in Table 3 and the renewed second order polynomial equation listed in Table 4 are approximately identical. The crack length values predicted from the renewed equation are in reasonable agreement with the experimental data (Table 5). The treated tracks, CP0850F05V1 and CP1000F05V1, prepared using process parameters close to the optimized parameters determined from the renewed second order polynomial equation listed in Table 4, have fewer cracks and are, even, free of macro-cracks when observed by eye, although that some micro-cracks can be observed by SEM (Fig. 9). Also, if the crack length per unit surface area is used to specify the extent of cracks, the trends in the crack length per unit surface area as a function of the investigated process parameters reflected by the regressed equations can be closely correlated with evolution of the phases and microstructures of the treated tracks with respect to the process parameters, as discussed in the following.

As for laser surface melting of similar refractory ceramics,[2–4] when the laser power is high enough, the extent of cracks decreases with decreasing workpiece traverse velocity. This is because a slower workpiece velocity tends to decrease the cooling and solidifying rates of the corresponding melt pool and, hence, decrease the thermal-induced stresses to some extent. A slower workpiece traverse velocity corresponding to lower cooling and solidifying rates of the melt pool can be directly confirmed from the microstructures of the treated tracks, shown in Figs. 9 and 10. The treated track produced using a slower workpiece traverse velocity (Fig. 9) obviously has a coarser microstructure than that produced using a faster workpiece traverse velocity (Fig. 10). A laser power greater than 1015 W would tend to increase the crack length per unit surface area with further increase in the laser power; this could be related to the fact that a high laser energy may produce larger temperature gradients and, hence, larger thermal stresses across the treated track.[2–4] In addition to the thermally induced stress, a stress resulting from changes in volume during the phase transformation of γ-Al_2O_3 to α-Al_2O_3 during solidification of the melt pool could be a more important factor in generating cracks. It has been found, from identification of the phase constituents of treated tracks using the XRD method, not reported here, that the sequence of alumina phases formed from melt pool during the combined processing is $\gamma \rightarrow \delta \rightarrow \theta \rightarrow \alpha$. According to theoretical density values of the various alumina phases,[16] there is about 7% shrinkage in volume from γ-Al_2O_3 to α-Al_2O_3. Thus, a higher α-Al_2O_3 content in a treated track would be responsible for greater volume shrinkage and, thus, a larger shrinking stress. On the one hand, with a decrease in the α-Al_2O_3 content and an increase in the mullite content in the treated tracks, the shrinking stresses associated with the transformation of γ-Al_2O_3 to α-Al_2O_3 are reduced; on the other hand, the elongated and interlocked mullite grains, of high strength,[1] improve the resistance to thermally induced cracks. Both factors are consistent with the fact that the crack length per unit surface area decreases with decrease in the α-Al_2O_3 content in the treated tracks. XRD results have indicated that the α-Al_2O_3 content decreases and the mullite content of a treated track increases with increase in laser power and decrease in powder feed rate (Fig. 7). Therefore, the relationships between the extent of cracks and the investigated process parameters reflected by the regressed equations listed in Tables 3 and 4 can be reasonably correlated with the material characteristics of the treated tracks.

The invalidity of the present statistical approach when the crack density is chosen as the objective function is concluded from the fact that the regressed equations in Table 6 and the renewed regressed equations in Table 7 exhibit different and, even, opposite trends in the dependency of crack density on the process parameters; there is a significant difference between the experimental crack density and the value predicted from the renewed regressed equations (Table 8). This may be because the crack data measured under the optical stereomicroscope were close to the true values in terms of total crack length, but deviated in terms of the number of cracks in the treated tracks. Due to the resolution of the optical stereomicroscope, cracks shorter than 0.5 mm were neglected in the crack measurement procedure. Although shorter cracks can be measured on polished cross sections of the treated tracks using a SEM or an optical microscope with higher resolution, the resulting crack data, expressed as the crack length per unit area of the cross section and the crack density, became irregular when correlated with the investigated process parameters. This may be because some cracks in the polished cross sections result from cutting, grounding and polishing of the samples; this leads to further complexity in correlating the crack data with the process parameters. Thus, such data are not presented in the present paper.

Large pores along the interfaces or within the treated surface layers resulted from aggregation of pores in the molten substrates (Figs. 8–10). These large pores were mainly along the interfaces between the treated surface layers and the substrates. Such a distribution of large pores was similar to that observed in single laser melting of similar refractory ceramics.[19] Following the theoretical models* developed by Triantafyllidis et al.[19] for describing the final boundary porosity and pore size, these large pores could be attributed to pore coalescence and healing of small pores due to motion of bubbles in the laser-induced melt pools. Consequently, a higher laser energy density should lead to

relatively larger average radius and smaller average number of these larger pores per unit volume in the vicinity of the interfaces. However, the initial porosity and pore size distribution in the treated substrates were the predominate factors in such large pore formation, as predicted by Triantafyllidis et al.'s models.[19] On the one hand, an identical type of refractory substrate has been used for all the present treated samples. On the other hand, as a result that the mullite aggregates, 1–4 mm in size, in the as-received substrates were comparable to widths of the present laser-treated surface layers, the initial porosity and pore size distribution in the substrates varied largely between different cross sections of an identical treated sample. Thus, the porosity and pore size distribution were not characterized in the present work.

In addition, phases adjacent to the melt/substrate interfaces showed excellent bonding between the treated surface layers and the substrates (Figs. 8–10), which is necessary for improving the high-temperature performance of the refractory brick. When mullite was the main phase, the cristobalite contents of the treated surface layers were decreased or, even, eliminated, when compared with the as-received refractory brick (Figs. 3 and 7). This means that the residual cristobalite in the as-received refractory brick has reacted with the sprayed powder particles during processing.

5. Conclusion

A statistical approach involving statistical experiment design and regression analysis has been used to optimize the process parameters of a novel process combining flame spraying of 20 wt.% Cr_2O_3–80 wt.% Al_2O_3 and CO_2 laser surface modification for improving the surface performance of an aluminosilicate refractory brick, with emphasis on reduction in the formation of cracks during the processing. The statistical experiment was designed according to a relatively new statistical experiment method, the uniform design experiment, in association with several experimental trials. The experimental crack data for the as-treated surface tracks were measured with an optical stereomicroscope. The regression analysis was carried out using the stepwise regression method to correlated the crack data with the investigated process parameters: laser power, powder feed rate and workpiece traverse velocity.

It was found that the present statistical approach is valid for optimizing the process parameters to achieve a reduction in the formation of cracks if the crack length per unit surface area is chosen as the objective function, but is invalid if the crack density is chosen as the objective function. The renewed second regressed equation for the crack length per unit surface area showed that, within the ranges used for the process parameters, the lower are the powder feed rate and the workpiece traverse velocity, the smaller is the crack length per unit surface area of the treated track. Under a low powder feed rate of 3.2 g/min and workpiece traverse velocity of 1 mm/s, the crack length per unit surface area decreases to a minimum value of 0.11 mm/mm^2 with increase in the laser power to 1015 W, then increases with further increase in the laser power. The treated tracks, prepared using process parameters close to the optimized parameters determined by the renewed second order polynomial equation of the crack length per unit surface area, contain fewer cracks and are, even, free of macro-cracks when observed by the human eye, even though some micro-cracks can be observed by SEM.

When the crack length per unit surface area was used as the measure of the extent of cracks, the renewed second regressed equation of the crack length per unit surface area could be correlated with the evolution of phases and microstructures in the treated tracks with respect to the process parameters. This was because reducing the powder feed rate corresponded to decreasing the α-Al_2O_3 content in the treated tracks; this could effectively reduce the stress resulting from volume changes during the transformation of γ-Al_2O_3 to α-Al_2O_3 during solidification of the melt pool. Decreasing the workpiece traverse velocity corresponded to decreasing the cooling and solidifying rates of the melt pool, and, thus, the thermally induced stress; this has been confirmed from the obviously coarser microstructure of the treated track produced using a slower workpiece traverse velocity than that produced using a faster workpiece traverse velocity.

Acknowledgements

The authors are grateful for the funding provided by the EPSRC (Grant Ref. GR/N08124). The authors are also grateful to Mr. D. Moore of the UMIST Corrosion and Protection Centre and Ms. J. Shackleton of the UMIST Materials Science Centre for their help with SEM examinations and XRD analysis, respectively.

References

1. Lee, W. E. and Rainforth, W. M., *Ceramic Microstructures: Property Control by Processing*. Chapman & Hall, London, UK, 1994, pp. 452–507.
2. Bradley, L., Li, L. and Stott, F. H., Flame-assisted laser surface treatment of refractory materials for crack-free densification. *Mater. Sci. Eng.* 2000, **A278**, 204–212.
3. Triantafyllidis, D., Li, L. and Stott, F. H., The combination of two laser energy sources for surface modification of high alumina ceramics. In *Congress Proceedings—Laser Materials Processing Conference and Laser Microfabrication Conference*. Laser Institute of America, 2001, pp. 158–167.
4. Triantafyllidis, D., Li, L. and Stott, F. H., Surface treatment of alumina-based ceramics using combined laser sources. *Appl. Surf. Sci.* 2002, **186**, 140–144.
5. Zhang, S., Rezaie, H. R., Sarpoolaky, H. and Lee, W. E., Alumina dissolution into silicate slag. *J. Am. Ceram. Soc.* 2000, **83**, 897–903.

6. Sandhage, K. H. and Yurek, G. J., Indirection dissolution of (Al, $Cr)_2O_3$ in CaO-MgO-Al_2O_3-SiO_2 (CMAS) melts. *J. Am. Ceram. Soc.* 1991, **74**, 1941–1954.
7. Fang, K. T. and Wang, Y., *Number-Theoretic Methods in Statistics*. Chapman & Hall, London, UK, 1993.
8. Kingswell, R., Scott, K. T. and Wassell, L. L., Optimizing the vacuum plasma spray deposition of metal, ceramic, and cermet coatings using designed experiments. *J. Therm. Spray Technol.* 1993, **2**, 179–186.
9. Li, C. J., Ji, G. C. and Wang, Y. Y., Effect of powder type on the relationship between spray parameters and properties of HVOF sprayed Cr_3C_2-NiCr coatings. In *Thermal Spray: Meeting the Challenges of the 21st Century*, ed. C. Coddet. ASM International, Materials Park, OH, 1998, pp. 278–292.
10. Montgomery, D. C., *Design and Analysis of Experiments*. John Wiley & Sons, New York, USA, 1997, pp. 536–642.
11. Christensen, R., *Analysis of Variance, Design and Regression*. Chapman & Hall, London, UK, 1996, pp. 426–434.
12. Li, J. F., Li, L. and Stott, F. H., Combined laser and flame surface coating of refractory ceramics-phase and microstructure characteristics. *Thin Solid Films* 2004, **453–454**, 229–233.
13. Herrmann, H. J., In *Fractals and Disordered Systems*, ed. A. Bunde and S. Havlin. Springer-Verlag, Berlin Heidelberg, Germany, 1991, pp. 175–206.
14. Krishnan, R., Dash, S., Rao, C. B., Rao, R. V. S., Tyagi, A. K. and Raj, B., Laser induced structural and microstructural transformations of plasma sprayed Al_2O_3 coatings. *Scripta Materialia* 2001, **45**, 693–700.
15. Ouyang, J. H., Nowtony, S., Richter, A. and Beyer, E., Characterization of laser clad yttria partially-stabilized ZrO_2 ceramic layers on steel 16MnCr5. *Surf. Coat. Technol.* 2001, **137**, 12–20.
16. JCPDS-International Centre for Diffraction Data, 1999, PDF 29-0063 & 42-1484.
17. Roth, R. S., Negas, T., Cook, L. P. and Smith, G., *Phase Diagrams for Ceramists, Vol 6*. American Ceramic Society, Westerville, Ohio, USA, 1987, Figs. 6442–6450.
18. Roth, R. S., Dennis, J. R. and McMurdie, H. F., *Phase Diagrams for Ceramists, Vol 4*. American Ceramic Society, Columbus, Ohio, USA, 1981, Fig. 5189.
19. Triantafyllidis, D., Li, L. and Stott, F. H., Mechanisms of porosity formation along the solid/liquid interface during laser melting of ceramics. *Appl. Surf. Sci.* 2003, **186**, 458–462.